SINTEF
PROCEEDINGS
2

Proceedings of the 12th International Conference on Computational Fluid Dynamics in the Oil & Gas, Metallurgical and Process Industries

Progress in Applied CFD – CFD2017

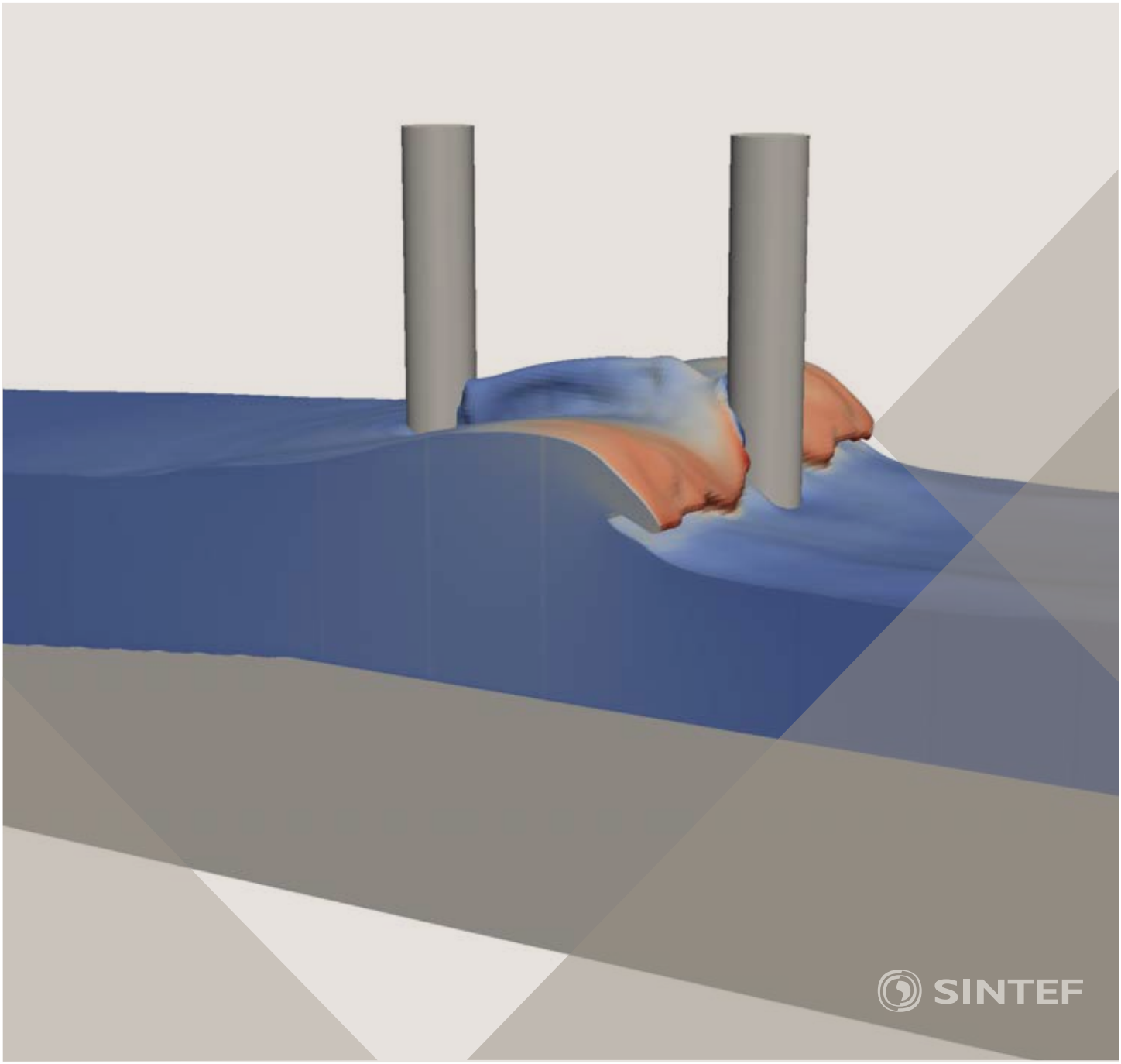

SINTEF Proceedings

Editors:
Jan Erik Olsen and Stein Tore Johansen

Progress in Applied CFD – CFD2017

Proceedings of the 12th International Conference on Computational Fluid Dynamics in the Oil & Gas, Metallurgical and Process Industries

SINTEF Academic Press

SINTEF Proceedings no 2
Editors: Jan Erik Olsen and Stein Tore Johansen
Progress in Applied CFD – CFD2017
Selected papers from 10th International Conference on Computational Fluid Dynamics in the Oil & Gas, Metallurgical and Process Industries

Key words:
CFD, Flow, Modelling

Cover, illustration: Arun Kamath

ISSN 2387-4295 (online)
ISBN 978-82-536-1544-8 (pdf)

SINTEF Academic Press
Address: Forskningsveien 3 B
PO Box 124 Blindern
N-0314 OSLO
Tel: +47 73 59 30 00
Fax: +47 22 96 55 08

www.sintef.no/byggforsk
www.sintefbok.no

SINTEF Proceedings
SINTEF Proceedings is a serial publication for peer-reviewed conference proceedings on a variety of scientific topics.
The processes of peer-reviewing of papers published in SINTEF Proceedings are administered by the conference organizers and proceedings editors. Detailed procedures will vary according to custom and practice in each scientific community.

PREFACE

This book contains all manuscripts approved by the reviewers and the organizing committee of the 12th International Conference on Computational Fluid Dynamics in the Oil & Gas, Metallurgical and Process Industries. The conference was hosted by SINTEF in Trondheim in May/June 2017 and is also known as CFD2017 for short. The conference series was initiated by CSIRO and Phil Schwarz in 1997. So far the conference has been alternating between CSIRO in Melbourne and SINTEF in Trondheim. The conferences focuses on the application of CFD in the oil and gas industries, metal production, mineral processing, power generation, chemicals and other process industries. In addition pragmatic modelling concepts and bio-mechanical applications have become an important part of the conference. The papers in this book demonstrate the current progress in applied CFD.

The conference papers undergo a review process involving two experts. Only papers accepted by the reviewers are included in the proceedings. 108 contributions were presented at the conference together with six keynote presentations. A majority of these contributions are presented by their manuscript in this collection (a few were granted to present without an accompanying manuscript).

The organizing committee would like to thank everyone who has helped with review of manuscripts, all those who helped to promote the conference and all authors who have submitted scientific contributions. We are also grateful for the support from the conference sponsors: ANSYS, SFI Metal Production and NanoSim.

Stein Tore Johansen & Jan Erik Olsen

Organizing committee:

Conference chairman: Prof. Stein Tore Johansen
Conference coordinator: Dr. Jan Erik Olsen
Dr. Bernhard Müller
Dr.Sigrid Karstad Dahl
Dr.Shahriar Amini
Dr.Ernst Meese
Dr.Josip Zoric
Dr.Jannike Solsvik
Dr.Peter Witt

Scientific committee:

Stein Tore Johansen, SINTEF/NTNU
Bernhard Müller, NTNU
Phil Schwarz, CSIRO
Akio Tomiyama, Kobe University
Hans Kuipers, Eindhoven University of Technology
Jinghai Li, Chinese Academy of Science
Markus Braun, Ansys
Simon Lo, CD-adapco
Patrick Segers, Universiteit Gent
Jiyuan Tu, RMIT
Jos Derksen, University of Aberdeen
Dmitry Eskin, Schlumberger-Doll Research
Pär Jönsson, KTH
Stefan Pirker, Johannes Kepler University
Josip Zoric, SINTEF

CONTENTS

SIMULATION OF CHEMICAL LOOPING COMBUSTION IN A DOUBLE LOOPING FLUIDIZED BED REACTOR WITH CU-BASED OXYGEN CARRIERS

Yuanwei ZHANG[1*], Øyvind LANGØRGEN[2†], Inge SAANUM[2‡], Zhongxi CHAO[3§], Hugo A. JAKOBSEN[1¶]

[1]NTNU Department of Chemical Engineering, 7034 Trondheim, NORWAY

[2]SINTEF Energy Research, Sem Sælands vei 11, 7034 Trondheim, Norway

[3]Safetec Nordic AS, 7037 Trondheim, Norway

[*] E-mail: yuanwei.zhang@ntnu.no
[†] E-mail: oyvind.langorgen@sintef.no
[‡] E-mail: inge.saanum@sintef.no
[§] E-mail: zhongxi.chao@safetec.no
[¶] E-mail: hugo.a.jakobsen@ntnu.no

ABSTRACT

Chemical looping combustion (CLC) is an attractive technology that produces a pure CO_2 stream and therefore the CO_2 can be readily recovered by condensing water vapour. In order to understand the physical phenomena and to explore the chemical process performance of the CLC process, a CFD model has been developed. The model is implemented numerically in an in-house code including the kinetic theory of granular flow and reaction models. Methane is used as fuel and CuO is chosen as oxygen carrier. This process is configured with an air reactor and a fuel reactor. The two reactors are simulated by a sequential approach. The connection between the two reactors is realized through time-dependent inlet and outlet boundary conditions. The widely used drag models were selected to examine their effects on the flow behaviour. The results indicating that the cluster effect in the FR is higher than in the AR. The frequency factor in the reaction model was varied to fit with the experimental measurements. The predicted result with the frequency factor of 1.35×10^{-3} gives a reasonable prediction in comparison to the experimental data.

Keywords: CFD, Double loop circulating fluidized bed, Drag model, Reactive flow .

NOMENCLATURE

Greek Symbols

α_k	Volume fraction of phase k, $[-]$
β	Inter-phase momentum transfer coefficient, $[\mathrm{kg/m^3 s}]$
γ_s	Collisional energy dissipation, $[\mathrm{J/m^3 s}]$
Γ	Interfacial mass transfer rate, $[\mathrm{kg/m^3 s}]$
ε_g	Turbulent energy dissipation rate, $[\mathrm{m^2/s^3}]$
Θ	Granular temperature, $[\mathrm{m^2/s^2}]$
κ_s	Conductivity of granular temperature, $[\mathrm{kg/ms}]$
λ_k	Thermal conductivity of phase k, $[\mathrm{m^2/s}]$
μ_k	Viscosity of phase k, $[\mathrm{kg/ms}]$
ν_j	Stoichiometric coefficient, $[-]$
ρ_k	Density of phase k, $[\mathrm{kg/m^3}]$
ρ_M	Molar density, $[\mathrm{mol/m^3}]$
τ	Time for complete solid conversion, [s]
$\bar{\bar{\tau}}_k$	Stress tensor of phase k, $[\mathrm{N/m^2}]$
$\bar{\bar{\tau}}_t$	Turbulent stress tensor, $[\mathrm{N/m^2}]$
ω	Mass fraction, $[-]$

Latin Symbols

A	Frequency factor, $[\mathrm{mol^{1-n} m^{3n-2}/s}]$.
C	Gas concentration, $[\mathrm{mol/m^3}]$.
C_1, C_2, C_b, C_μ	Turbulence model parameter, $[-]$.
C_d	Drag coefficient, $[-]$.
d_s	Particle diameter, [m].
D_{ji}	Binary diffusion coefficient, $[\mathrm{m^2/s}]$.
$D_{k,j}$	Diffusion coefficient for component j in phase k, $[\mathrm{m^2/s}]$.
e_{ss}	Particle restitution coefficient, $[-]$.
E	Activation energy, $[\mathrm{kJ/mol}]$.
$\vec{g}$	Gravity acceleration, $[\mathrm{m/s^2}]$.
g_0	Radial distribution function, $[-]$.
$\bar{\bar{\mathrm{I}}}$	Unit tenser, $[-]$.
k	Reaction rate coefficient, $[\mathrm{mol^{1-n} m^{3n-2}/s}]$.
k_g	Gas turbulent kinetic energy, $[\mathrm{m^2/s^2}]$.
K	Scale factor, $[-]$.
$\vec{M}_k$	Interfacial momentum transfer, $[\mathrm{kg/m^2 s^2}]$.
M	Mole mass, $[\mathrm{kg/kmol}]$.
n	Reaction order, $[-]$.
p_k	Pressure of phase k, [Pa].
Pr	Prandtl number, $[-]$.
r	Reaction rate, $[\mathrm{mol/m^3 s}]$.
r_g	Radius of a grain, [m].
R	Gas constant, $[\mathrm{J/mol^{-1} K^{-1}}]$.
Re_p	Particle Reynolds number, $[-]$.
S_t	Turbulent kinetic energy production, $[\mathrm{kg/ms^3}]$.
t	Time, [s].
T	Temperature, [K].
$\vec{v}_k$	Velocity of phase k, $[\mathrm{m/s}]$.
V_M	Molar colume, $[\mathrm{m^3/mol}]$.
X	Gas conversion, $[-]$.
z	Axial coordinate, [m].

Sub/superscripts

0	Initial.
B	Bulk.
$dilute$	Dilute.
e	Effective.
g	Gas.
i	Reaction number.
k	Gas ($k = g$) or solid ($k = s$) phase.
m	Molecular.
max	Maximum.
mf	Minimum fluidization.
s	Solid.
t	Turbulent.

INTRODUCTION

Chemical-looping combustion (CLC) is an efficient and low cost combustion process that can be explored to limit CO_2 emissions. This new type of combustion is a two-step combustion process. Typically, it consists of two interconnected fluidized bed reactors, the fuel reactor and the air reactor. A solid oxygen carrier (OC) gets oxidized and reduced in a cyclic manner, carrying the oxygen from one reactor to he other. First, the fuel is introduced to the FR and reacts with the oxidized OC, to give CO_2 and steam. The oxidized OC being reduced from MeO_α to $MeO_{\alpha-1}$. In a subsequent step, this oxygen carrier is reoxidized to its initial state with air in the AR, from $MeO_{\alpha-1}$ to MeO_α. The overall reaction obtained summing the oxidation and reduction of the OC is equivalent to the conventional combustion of the fuel and relases exactly the same amount of energy. Since the mixing of fuel and air is avoided, CO_2 will inherently not be diluted with nitrogen (Ishida and Jin, 1996).

In order to get sufficiently high fuel conversion, enhance gas-solid contact and realize flexible operation, SINTEF Energy Research and the Norwegian University of Science and Technology have designed a double loop circulating fluidized bed (DLCFB) reactor for the CLC process, as shown in Figure 1. The design is sized to be used with gaseous fuel. It consists of two circulating fluidized beds interconnected by means of divided loop seals and a bottom extraction. The fluidizing gas (methane in the FR and air in the AR) is fed from bottom of the reactors. The solid outflow from one reactor will inject into the bottom of the other reactor through the cyclones and divided loop seals. The propose of the divided loop seal is both to avoid the gas mixing between the two reactors and to lead flow of solids entrained by one reactor into the other one or recirculate it back to the reactor of origin. The air reactor as well as the fuel reactor are operated in the turbulent or fast fluidization regime for a better gas-solid contact. This special design is meant to be flexible with respect to OCs and to be extrapolated to other chemical looping applications. In addition, the arrangement is compact in order to ease the up-scaling as well as for the prospective of pressurizing the reactor as a further step.

Computational fluid dynamics (CFD) is expected to play an important role in studying the hydrodynamic and chemical process performance of gas-solid system. In order to understand the physical phenomena, explore the reactive performance of the CLC process in the DLCFB system, it is beneficial to develop a simulation model, which further can be used to optimize the operating conditions, and for scale-up and design of industrial scale reactors.

In this work, a reactive multiphase CFD model for an interconnected DLCFB reactor has been developed and implemented using an in-house Fortran code. Euler-Euler approach with the kinetic theory of granular flow (KTGF) has been selected. Methane is used as the gaseous fuel and CuO is chosen as OC. The main objective of this investigation is to validate the model based on the real experimental data and make preparation for the further research.

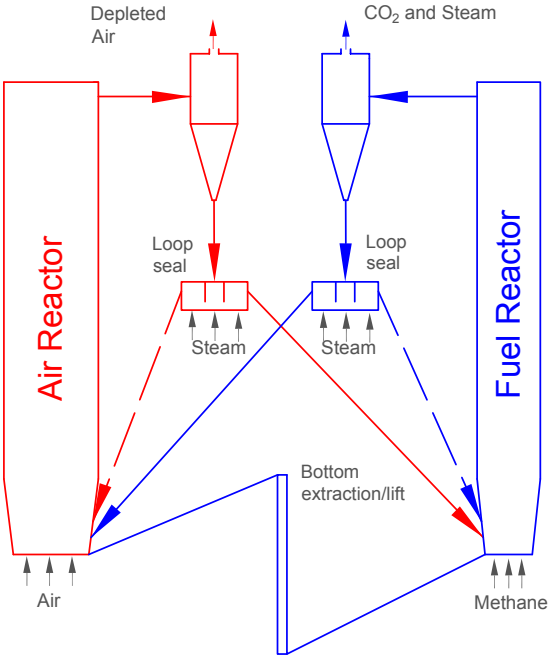

Figure 1: Sketch of the DLCFB reactor.

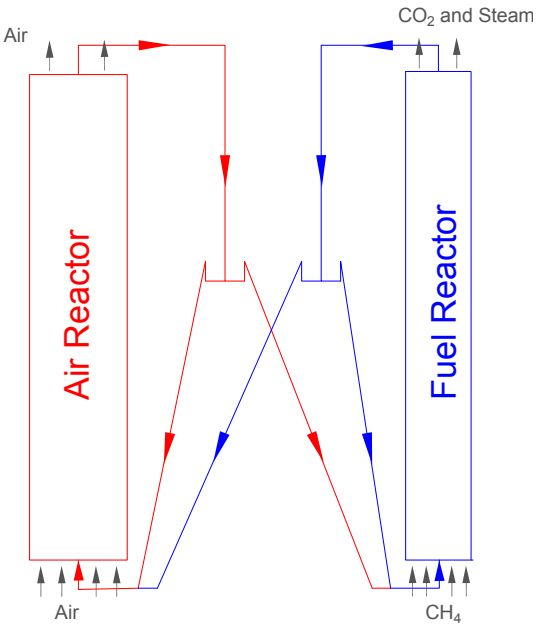

Figure 2: Sketch of the DLCFB reactor.

MODEL DESCRIPTION

A two-fluid reactive flow model based on the KTGF implemented in an in-house code is used to describe the hydrodynamics and the reacting system in the fluidized reactors. In the two-fluid model, each phase is described by a set of governing equations and closures. For the gas phase, the transport equations can be derived by adopting suitable averaging process for local instantaneous equations, while the transport

equations for solid phase originate from the ensemble average of a single-particle quantity over the Boltzmann integral-differential equation. Detailed descriptions of the model can be found in (Jakobsen, 2014). The governing equations are summarised in Table 1. The standard $\kappa-\varepsilon$ turbulence model is chosen for characterizing the gas phase turbulence phenomena, the corresponding closure models are shown in Tables 2 and 3. The KTGF is adopted to derive the physical properties of solid phase by introducing the granular temperature, Θ. The two phases are coupled through the interfacial momentum transfer, which is dominated by the drag force. In this study, the most commonly used drag coefficient models proposed by Gidaspow(Gidaspow, 1994), Syamlal and O'Brien(Syamlal and O'Brien, 1988) and Gibilaro(Gibilaro *et al.*, 1985) are selected to examine their influence on the simulated results. In addition, McKeen and Pugsley(McKeen and Pugsley, 2003) model was used for accounting the cluster effect. The description of the drag models are given in the Appendix A. The internal phases constitutive equations are listed in Tables 4 and 5.

The oxygen carrier material used in the simulation is a coper oxide based material with a CuO content of 14.7 %. The particle density and diameter are 1700 $\mathrm{Kg/m^3}$ and 149 μm respectively. One step reactions are assumed both for the fuel and air reactors and given as follows:

$$4\mathrm{CuO}+\mathrm{CH_4}\rightarrow\mathrm{CO_2}+2\mathrm{H_2O}+4\mathrm{Cu} \tag{1}$$

$$2\mathrm{Cu}+\mathrm{O_2}\rightarrow 2\mathrm{CuO} \tag{2}$$

The particle was assumed to be composed by spherical grains of CuO. The shrinking core model (SCM) with the reaction controlled by the chemical reaction in the grain was applied. The equations that describe the reaction model are follows(Abad *et al.*, 2007):

$$X=\frac{t}{\tau} \tag{3}$$

where X is the degree of conversion, τ is the time for complete conversion of the carrier and is calculated from:

$$\tau=\frac{r_{g,\mathrm{CuO}}}{\nu V_{M,\mathrm{CuO}} k C^n} \tag{4}$$

C, n, ν, r_g and V_M represent the concentration of the gas reactant, reaction order, stoichiometric factor, mean radius of the grains, and molar volume, respectively. The reaction constant k follows:

$$k=A\exp(-E/RT) \tag{5}$$

where A is the pre-exponential factor of the rate constant, also known as the frequency factor. E is the activation energy, and R is the constant of the ideal gas ($R=8.314\mathrm{J/mol^{-1}K^{-1}}$).

The reaction rate of equation 1 and 2 is expressed as follows:

$$(-r)_i=\left(\frac{\rho_{M,\mathrm{CuO}}\alpha_s\omega_{\mathrm{CuO}}}{\nu}\frac{\mathrm{d}X}{\mathrm{d}t}\right)_i \tag{6}$$

where i and ρ_M represent the ith reaction and molar density. The detailed kinetic parameters are listed in table 6(Abad *et al.*, 2007).

The source term in the species mass balance equation for the j th species in the gas can be modelled by:

$$\Gamma^{\omega}_{g,j}=\nu_j M_j r \tag{7}$$

The mass transfer between the gas phase and the solid phase is calculated as following the relation proposed by Jung and Gamwo (Jung and Gamwo, 2008):

$$\Gamma_g=\nu_{\mathrm{O_2}}M_{\mathrm{O_2}}r=-\Gamma_s \tag{8}$$

Numerical implementation of the coupling between reactors

The chemical looping combustion process is simulated by utilizing the DLCFB system as described above. A 2D plane geometry is chosen for the simulation of the fuel and air reactors, which is shown in Figure 2, having the same dimensions as the experimental setup. The computational domain is meshed by using uniform grids in each direction.

Two different sets of coordinates and parameters are adopted to solve the governing equations for the AR and the FR respectively. The solid flowing out of the AR is fed into the bottom of the FR, and in a similar way all the solids that exited at the outlet of FR will be injected into the bottom of the AR. The exchange of the solid flow between the reactor units is realized through the time-dependent inlet and outlet boundary conditions. At each simulation time step, the processes in the two risers are simulated by a sequential approach, the solid flux of the inlet of one riser is calculated from the solid flowing out of the outlet of the other riser with the same OC condition. In the experiment, this kind of continuous solid exchange is achieved by means of cyclones, divided loop-seals and the bottom lift. The cyclones are neglected in the simulation by assuming the efficiency of the cyclones are equal to one. The bottom extraction/lift is replaced by an internal recirculation mechanism in order to keep the mass balance inside each reactor. In this way, a full loop is fulfilled for one time step. Then, another computation loop for next time step will run repeatedly.

Initial and boundary condition

Initially, there is no gas flow in the reactor and the bed is at rest with a particle volume fraction of 0.4. A uniform plug gas flow is applied at the inlets of the reactors, the inlet solid flux of one of the reactors is kept consistent with the outlet solid flux of the other one with a prescribed solid volume fraction at the inlet. The normal velocities at all boundaries are set to zero. No-slip wall boundary condition is set for the gas phase while the solids are allowed to slip along the wall, following the equation (9) from (Jakobsen, 2014).

$$\vec{v}_{s,z}|_{wall}=\frac{d_s}{\alpha_s^{1/3}}\frac{\partial\vec{v}_{s,z}}{\partial r} \tag{9}$$

where $\vec{v}_{s,z}$ is the axial velocity of the particles. r denotes the direction normal to the wall.

For all the scalar variables but pressure, Dirichlet boundary conditions are used at the inlets, while Neumann conditions are used at the other boundaries. For the pressure correction equations, all the boundaries except outlet, Neumann conditions are adopted. At the outlet a fixed pressure (101325 Pa) is specified.

Numerical Procedure

The two-fluid model equations are discretized by finite volume method and implemented in a Fortran program. The algorithm is based on the work by Lindborg (Lindborg, 2008) and Jakobsen(Jakobsen, 2014). The second order central differential scheme is used to discretize the diffusion terms. In order to reduce the oscillation and keep higher-order accuracy of the numerical solution, a total variation diminishing

(TVD) scheme is employed for discretizing the convention term (van Leer, 1974). In this scheme, cell face values are calculated from the combination of upwind scheme part and a suitable anti-diffusive part, which controlled by a smoothness function. In this way, a higher-order discretization scheme is used in smooth regions and reduce to the first order at local extrema of the solution. The upwind part is treated fully implicitly while the anti-diffusive part is treated explicitly. The SIMPLE algorithm for multiphase flow is selected for the pressure-velocity coupling (Jakobsen, 2014). Due to the strong coupling of the two phases, the coupling terms are handled specially in the discretized transport equations, and then the coupled equations are solved simultaneously by using a coupled solver. The species mass balance equations are solved by applying a fractional step scheme which decouples the chemistry (i.e., kinetics) and the transport (i.e., convection and diffusion) terms. All the linear equation systems are solved by the preconditioned Bi-conjugate gradient (BCG) algorithm (Lindborg, 2008).

RESULTS

The chemical looping combustion experiments have been conducted in the DLCFB system at SINTEF Energy Research in Trondheim. Pressure transducers were placed along the reactor bodies to measure the local pressure distribution. CH_4, CO_2 and O_2 concentration were measured in the exhaust from the FR and the AR. The operating and initial conditions of the simulation are adopted the same as the actual experiment, summarized in Table 8. The first part of this section presents the validation of the hydrodynamics and reactive model by using different drag models. Then the chemical process performances were analysed. The simulations were conducted for 20 seconds of real time. To ensure the initial transient effects are not included in the analysis, the last 10 seconds of the simulations are used for extracting the mean results.

Verification of the hydrodynamic model

For the simulation procedure, grid sensitivity study was carried out in advance in previous work by Zhang et al (Zhang *et al.*, 2017). The drag model plays a critical role for the successful simulation of the hydrodynamics in a gas-solid system. Three widely used drag models were selected to examine their effects on the flow behaviour.

Figure 3 shows the predicted axial profiles of the pressure in the FR. The corresponding axial solid concentration distribution can be found in Figure 5. It can be seen that the Gidaspow(Gidaspow, 1994), Syamlal and O'Brien(Syamlal and O'Brien, 1988) models give nearly identical results, which are overestimate the inter-phase momentum transfer in the FR, and hence predict a more uniform distribution of solids across the riser. That is why the predicted pressure was far away from the experimental data, especially in the upper part of the reactor. The discrepancy was ameliorated a little by using the Gibilaro(Gibilaro *et al.*, 1985) model, but still overestimate the interphase drag force. This could be explained by the cluster effect inside the FR. The existence of cohesive interparticle forces would lead to grouping of particles, resulting in larger effective particle sizes, and hence reduced fluid-particle drag forces.

In order to account for the aggregation of particles, some modifications have been proposed. McKeen and Pugsley et al.(McKeen and Pugsley, 2003) proposed an empirical method to reduce the Gibilaro(Gibilaro *et al.*, 1985) drag correction using a constant scale factor, K. This scale factor

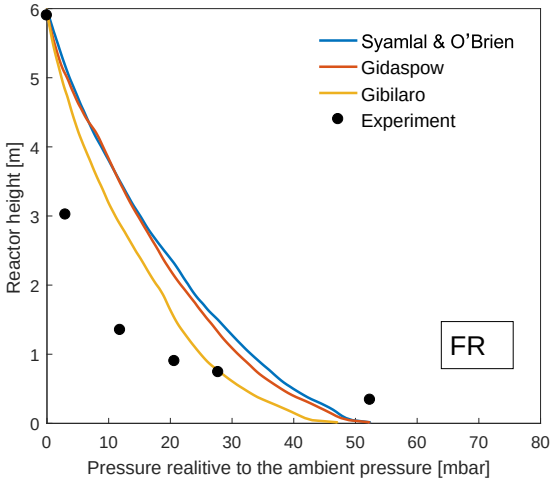

Figure 3: Axial pressure distribution.

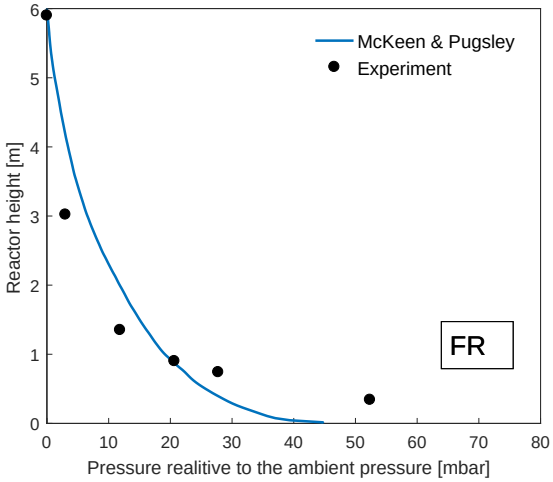

Figure 4: Axial pressure distribution.

could be adjusted to take in to account the effect of interparticle cohesive forces on particle agglomeration. In this study, the scale factor is set to 0.6.

The predicted axial pressure and solid distribution with McKeen and Pugsley model(McKeen and Pugsley, 2003) shown in the Figure 4 and Figure 5 respectively. It can be seen that the predicted results calculated by McKeen and Pugsley model (McKeen and Pugsley, 2003) are in good agreement with the experimental data, except for the reasonable deviation occurring in the dense bottom zone, which can be mostly attributed to the incomplete 2-D description of a real 3-D geometry according to our numerical experiences. From Figure 5, the basic feature of the turbulent fluidization regime was achieve with coexisting the dilute and dense phase.

Figure 6 displays the predicted axial profiles of the pressure in the AR with aforementioned drag models. For the AR, the predicted result calculated by the Gibilaro(Gibilaro *et al.*, 1985) model shows the best agreement with the experimental data. However, the McKeen and Pugsley model(McKeen and Pugsley, 2003) underestimated the drag force. It should be pointed out that the inlet gas velocity in the AR is higher compared with FR due to the air to fuel ratio, which could result in the different fluidization regimes of the two reactors and hence lead to the different degrees of cluster effect. Besides, as the reactions go on, the particle density increases in the AR and decreases in the FR, which could be another factor to the difference of fluidization regimes of the FR and the

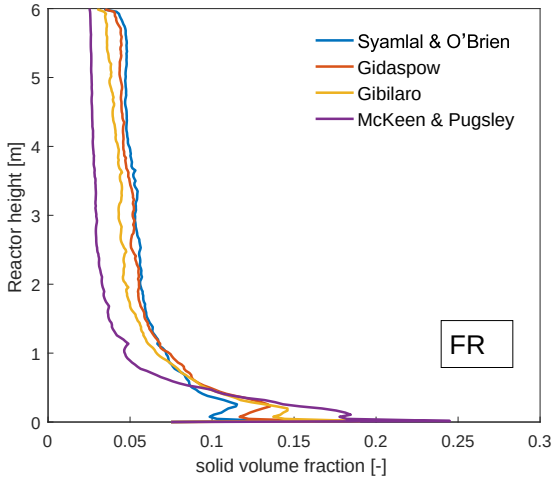

Figure 5: Axial solid volume fraction.

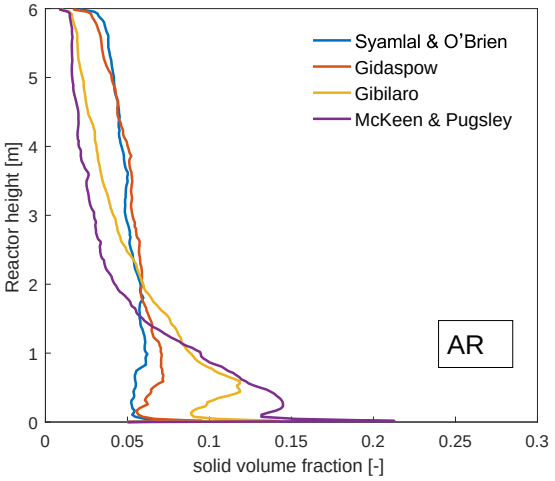

Figure 7: Axial solid volume fraction.

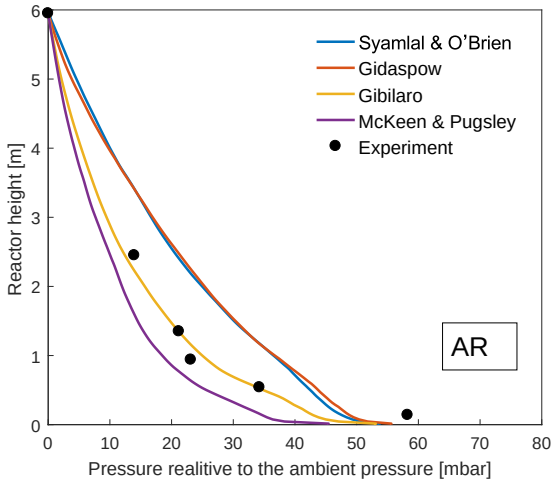

Figure 6: Axial pressure distribution.

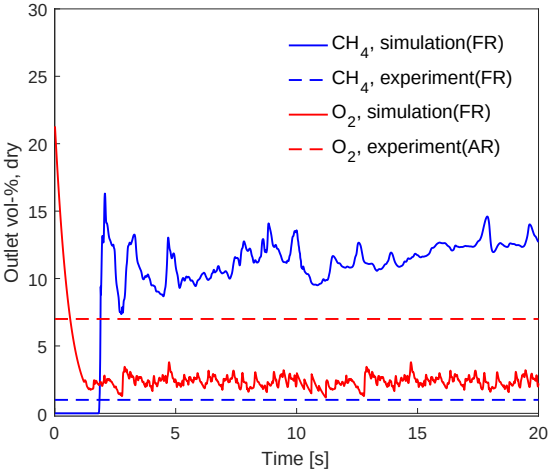

Figure 8: Concentration of CH_4 in the FR exhaust and O_2 concentration out from the AR.

AR. Since the Gibilaro (Gibilaro *et al.*, 1985) model gives reasonable prediction in the AR whereas overpredictes the drag force in the FR, it could be concluded that the degree of clustering in the FR is higher than in the AR. The corresponding solid distribution is shown in 7.

Verification of the chemical reaction model

In this section, the chemical reaction model was validated based on the experimental results of the CH_4 concentration in the fuel reactor exhaust as well as the O_2 concentration out from the air reactor.

Figure 8 displays the CH_4 and O_2 concentration calculated from the simulation and the measurements from the experiments. For both reactors, relatively stable outlet concentrations of the gas species are achieved in just a few seconds of simulation time, hence the reactive flow can be said to be at a quasi-steady-state. It can be observed that the predicted O_2 concentration agrees reasonably with the experiment data although the result is slight under-predicted. However, the predicted CH_4 concentration is far away from the experimental data. This can be explained as the CuO used in the current study is slight different from the literature (Abad *et al.*, 2007), which would lead to a certain amount of error of the kinetic parameters. So in order to match the experimental result, three more frequency factors (A, in equation 5) for reduction reaction were evaluated, as shown in Figure 9. The best agreement between the simulation result and the experimental data was found when the frequency factor was equal to 1.35×10^{-3}.

With a frequency factor of 1.35×10^{-3}, McKeen and Pugsley(McKeen and Pugsley, 2003) model in the FR and Gibilaro(Gibilaro *et al.*, 1985) model in the AR, the vertical profiles of gas concentration in both reactors are examined. As illustrated in Figure 10, the reactants, CH_4 and O_2, are rapidly consumed at a very short entrance length, where there is a larger concentration gradient. At the upper part of the reactors, the concentration gradient is much smaller. The reverse trend is observed for gas products CO_2.

CONCLUSION

The conclusions are:

1. The degree of clustering is higher in the FR than in the AR, which needs different drag models for each reactor. The predicted results given by McKeen and Pugsley(McKeen and Pugsley, 2003) model in the FR and Gibilaro(Gibilaro *et al.*, 1985) model in the AR show good agreement with the experimental data.

2. Due to the difference between the OC used in this study and the one for deriving the kinetic parameters, the frequency factor need to be modified according to the experimental measurements, andThe best agreement between the simulation result. The frequency factor of

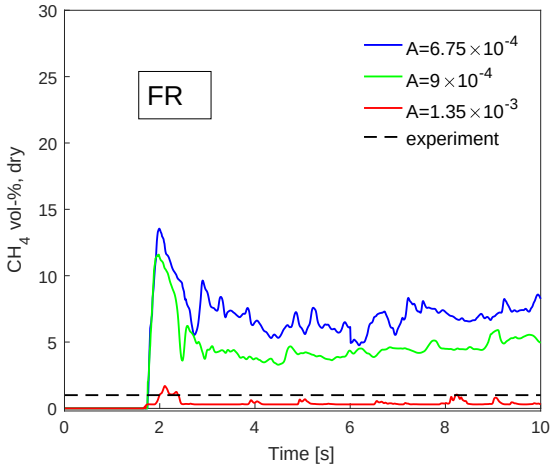

Figure 9: Concentration of CH_4 in the FR exhaust.

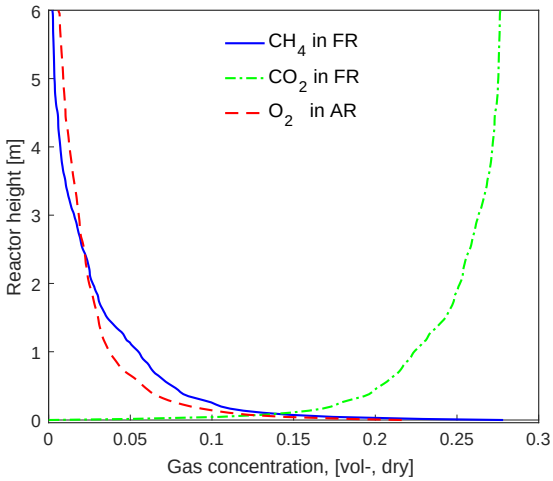

Figure 10: Axial distribution of CH_4,CO_2 and O_2 along the reactors.

Table 1: Governing equations.

(Jakobsen, 2014; Lindborg, 2008)

Continuity equation for phase k ($k = g,s$)

$$\frac{\partial}{\partial t}(\alpha_k\rho_k)+\nabla\cdot(\alpha_k\rho_k\vec{v}_k)=\Gamma_k$$

Momentum equation for phase k ($k = g,s$)

$$\frac{\partial}{\partial t}(\alpha_k\rho_k\vec{v}_k)+\nabla\cdot(\alpha_k\rho_k\vec{v}_k\vec{v}_k)=-\alpha_k\nabla p-\nabla\cdot\alpha_k\bar{\bar{\tau}}_k+\vec{M}_k+\alpha_k\rho_k\vec{g}+\Gamma_k^{\vec{v}}$$

Species mass balance for phase k ($k = g,s$)

$$\frac{\partial}{\partial t}(\alpha_k\rho_k\omega_{k,j})+\nabla\cdot(\alpha_k\rho_k\vec{v}_k\omega_{k,j})=\nabla\cdot(\alpha_k\rho_k D^e_{k,j}\nabla\omega_{k,j})+\Gamma^{\omega}_{k,j}$$

Gas turbulent kinetic energy equation

$$\frac{\partial}{\partial t}(\alpha_g\rho_g k_g)+\nabla\cdot(\alpha_g\rho_g k_g\vec{v}_g)=\alpha_g(-\bar{\bar{\tau}}_t:\nabla\vec{v}_g+S_t)+\nabla\cdot(\alpha_g\frac{\mu_g^t}{\sigma_g}\nabla k_g)-\alpha_g\rho_g\varepsilon_g$$

Gas turbulent energy dissipation rate equation

$$\frac{\partial}{\partial t}(\alpha_g\rho_g\varepsilon_g)+\nabla\cdot(\alpha_g\rho_g\varepsilon_g\vec{v}_g)=\alpha_g C_1\frac{\varepsilon_g}{k_g}(-\bar{\bar{\tau}}_t:\nabla\vec{v}_g+S_t)+\nabla\cdot(\alpha_g\frac{\mu_g^t}{\sigma_\varepsilon}\nabla\varepsilon_g)-\alpha_g\rho_g C_2\frac{\varepsilon_g^2}{k_g}$$

Granular temperature equation

$$\frac{3}{2}\left[\frac{\partial}{\partial t}(\alpha_s\rho_s\Theta_s)+\nabla\cdot(\alpha_s\rho_s\Theta_i\vec{v}_s)\right]=-\bar{\bar{\tau}}_s:\nabla\vec{v}_s+\nabla\cdot(\kappa_s\nabla\Theta_s)-3\beta\Theta_s-\gamma_s$$

Table 2: Closure for turbulent model

Turbulent viscosity

$$\mu_g^t=\rho_g C_\mu\frac{k_g^2}{\varepsilon_g}$$

Turbulent kinetic energy production(Jakobsen, 1993)

$$S_t=C_b\beta(\vec{v}_s-\vec{v}_g)^2$$

Turbulent stress tensor(Jakobsen, 2014)

$$\bar{\bar{\tau}}_t=-\frac{2}{3}\rho_g k_g\bar{\bar{I}}+2\mu_g^t\bar{\bar{S}}_g$$

Table 3: Empirical parameters for the $\kappa-\varepsilon$ model

(Jakobsen, 2014)

C_μ	σ_0	σ_ε	C_1	C_2	C_b
0.09	1.00	1.30	1.44	1.92	0.25

Table 4: Closure for internal momentum transfer

(Lun *et al.*, 1984; Gidaspow, 1994)

Gas phase stress

$$\bar{\bar{\tau}}_g=2\alpha_g\mu_g\bar{\bar{S}}_g$$

Solid phase stress

$$\bar{\bar{\tau}}_s=-(-p_s+\alpha_s\mu_{B,s}\nabla\cdot\vec{v}_s)-2\alpha_s\mu_s\bar{\bar{S}}_s$$

Deformation rate for phase k ($k = g,s$)

$$\bar{\bar{S}}_k=\frac{1}{2}\left(\nabla\vec{v}_k+(\nabla\vec{v}_k)^T\right)-\frac{1}{3}(\nabla\cdot\vec{v}_k)\bar{\bar{I}}$$

Solid phase pressure

$$p_s=\alpha_s\rho_s\Theta_s[1+2(1-e)\alpha_s g_0]$$

solid bulk viscosity

$$\mu_{B,s}=\frac{4}{3}\alpha_s\rho_s d_p g_0(1+e)\sqrt{\frac{\Theta_s}{\pi}}+\frac{4}{5}\alpha_s\rho_s d_p g_0(1+e)$$

Solid phase shear viscosity

$$\mu_s=\frac{2\mu_s^{dilute}}{\alpha_s g_0(1+e)}\left[1+\frac{4}{5}\alpha_s g_0(1+e)\right]^2+\frac{4}{5}\alpha_s\rho_s g_0(1+e)\sqrt{\frac{\Theta_s}{\pi}}$$

Conductivity of the granular temperature

$$\kappa_s=\frac{15}{2}\frac{\mu_s^{dilute}}{(1+e)g_0}\left[1+\frac{6}{5}\alpha_s g_0(1+e)\right]^2+2\alpha_s^2\rho_s d_p(1+e)g_0\sqrt{\frac{\Theta_s}{\pi}}$$

Collisional energy dissipation

$$\gamma_s=3(1-e^2)\alpha_s^2\rho_s g_0\Theta_s\left[\frac{4}{d_p}\sqrt{\frac{\Theta_s}{\pi}}-\nabla\cdot\vec{v}_s\right]$$

Radial distribution function

$$g_0=\frac{1+2.5\alpha_s+4.5904\alpha_s^2+4.515439\alpha_s^3}{\left[1-(\frac{\alpha_s}{\alpha_s^{max}})^3\right]^{0.67802}}$$

Dilute viscosity

$$\mu_s^{dilute}=\frac{5}{96}\rho_s d_p\sqrt{\pi\Theta_s}$$

Table 5: Constitutive equations for internal mass transfer

(Jakobsen, 2014; Lindborg, 2008)

Effective diffusivity

$$D^e_{k,j}=D^m_{k,j}+D^t_k$$

Molecular diffusion coefficient

$$D^m_{g,j}=\frac{1-\omega_j}{M_m\sum_{j\neq i}\frac{\omega_j}{M_j D_{ji}}}$$

Binary diffusion coefficient

$$D_{ji}=\frac{T_0^{1.75}\sqrt{1/M_j+1/M_i}}{101.325P\left((\sum V)_j^{1/3}+(\sum V)_i^{1/3}\right)^2}$$

Turbulent diffusion coefficient

$$D^t_g=\frac{\mu_g^t}{\rho_g Sc^t}$$

$$D^t_s=\frac{d_p}{16\alpha_s}\sqrt{\pi\Theta}$$

Table 6: Main geometric and operating parameters

(Abad *et al.*, 2007)

	CH_4	O_2
Physical parameters		
$\rho_{M,CuO}(mol/m^3)$	80402	80402
$r_{g,CuO}(m)$	1.4×10^{-6}	1.4×10^{-6}
ν	4	2
Kinetic parameters		
$A(mol^{1-n}m^{3n-2}s^{-1})$	4.5×10^{-4}	4.7×10^{-6}
$E(kJ/mol)$	60	15
n	0.4	1

Table 7: Main geometric and operating parameters

Description	Unit	Value
Reactor geometry		
AR height	m	6
AR diameter	m	0.23
FR height	m	6
FR diameter	m	0.154
Particle properties		
Mean particle size	μm	149
Particle density	kg/m^3	1700
Active NiO content	%	14.7
Operational condition		
Operating pressure	atm	1.0
Fuel power	kW	100
Lower heating value of fuel	MJ/kg	50
Inlet composition of FR	–	27 % CH_4
Temperature in FR	K	1100
Temperature in AR	K	1100
Global air-fuel ratio	–	1.1

Table 8: Main geometric and operating parameters

Description	Unit	Value
No. of control volume	–	22800
Gas viscosity	kg/ms	1.82×10^{-5}
Sphericity of particle	–	1
Restitution coefficient of particles	–	0.99
Initial bed height of FR	m	0.9
Initial bed height of AR	m	1.2
Time step	s	1.0×10^{-4}

1.35×10^{-3} gives a reasonable prediction in comparison to the experimental data.

REFERENCES

ABAD, A., ADÁNEZ, J., GARCÍA-LABIANO, F., LUIS, F., GAYÁN, P. and CELAYA, J. (2007). "Mapping of the range of operational conditions for cu-, fe-, and ni-based oxygen carriers in chemical-looping combustion". *Chemical Engineering Science*, **62(1)**, 533–549.

ERGUN, S. (1952). "Fluid flow through packed columns". *Chem. Eng. Prog.*, **48**, 89–94.

GIBILARO, L., DI FELICE, R., WALDRAM, S. and FOSCOLO, P. (1985). "Generalized friction factor and drag coefficient correlations for fluid-particle interactions". *Chemical engineering science*, **40(10)**, 1817–1823.

GIDASPOW, D. (1994). *Multiphase flow and fluidization: continuum and kinetic theory descriptions*. Academic press, San Diego, US.

ISHIDA, M. and JIN, H. (1996). "A novel chemical-looping combustor without nox formation". *Ind. Eng. Chem. Res.*, **35**, 2469–2472.

JAKOBSEN, H.A. (1993). *On the modelling and simulation of bubble column reactors using a two-fluid model*. Ph.D. thesis, Norwegian Institute of Technology, Trondheim, Norway.

JAKOBSEN, H.A. (2014). *Chemical Reactor Modeling*. 2nd ed. Springer-Verlag, Multiphase Reactive Flows, Berlin, Germany: Springer-Verlag.

JUNG, J. and GAMWO, I.K. (2008). "Multiphase cfd-based models for chemical looping combustion process: fuel reactor modeling". *Powder Technol.*, **183(3)**, 401–409.

LINDBORG, H. (2008). *Modeling and Simulation of Reactive Two-Phase Flows in Fluidized Bed Reactors*. Ph.D. thesis, Norwegian Institute of Technology, Trondheim, Norway.

LUN, C., SAVAGE, S.B., JEFFREY, D. and CHEPURNIY, N. (1984). "Kinetic theories for granular flow: inelastic particles in couette flow and slightly inelastic particles in a general flowfield". *J. Fluid Mech.*, **140**, 223–256.

MCKEEN, T. and PUGSLEY, T. (2003). "Simulation and experimental validation of a freely bubbling bed of fcc catalyst". *Powder Technol.*, **129(1)**, 139–152.

SYAMLAL, M. and O'BRIEN, T. (1988). "Simulation of granular layer inversion in liquid fluidized beds". *International Journal of Multiphase Flow*, **14(4)**, 473–481.

VAN LEER, B. (1974). "Towards the ultimate conservation difference scheme. ii. monotonicity and conservation combined in a second-order scheme". *J. Comput. Phys.*, **14**, 361–370.

WEN, C. and YU, Y. (1966). "A generalized method for predicting the minimum fluidization velocity". *AIChE Journal*, **12(3)**, 610–612.

ZHANG, Y., CHAO, Z. and JAKOBSEN, H.A. (2017). "Modelling and simulation of hydrodynamics in double loop circulating fluidizedbed reactor for chemical looping combustion process". *Powder Technology*, **310**, 35–45.

APPENDIX A

The drag force acting on a particle in gas-solid system can be presented by the product of a momentum transfer coefficient (β) and slip velocity between the two phases

$$\vec{M} = \frac{3}{4} C_d \frac{\alpha_s \rho_g}{d_s} f(\alpha_g) |\vec{u}_g - \vec{u}_s| = \beta(\vec{u}_s - \vec{u}_g) \qquad (A.1)$$

The correlations of β are usually obtained from pressure drop measurements.
Gidaspow et al.(Gidaspow, 1994) employed the Ergun (Ergun, 1952) equation for the dense phase and the Wen-Yu (Wen and Yu, 1966) equation for the dilute phase.

$$\beta = \begin{cases} 150\frac{\mu_g(1-\alpha_g)^2}{\alpha_g d_s^2} + 1.75(1-\alpha_g)\frac{\rho_g}{d_s}|\vec{u}_g - \vec{u}_s| & \alpha_g < 0.8 \\ 0.75 C_d \frac{(1-\alpha_g)\alpha_g}{d_s}\rho_g |\vec{u}_g - \vec{u}_s| \alpha_g^{-2.65} & \alpha_g > 0.8 \end{cases} \qquad (A.2)$$

where the drag coefficient C_D was expressed by

$$C_d = \begin{cases} \frac{24}{Re_p}[1 + 0.15 Re_p^{0.687}] & Re_p \le 1000 \\ 0.44 & Re_p > 1000 \end{cases} \qquad (A.3)$$

The particle Reynolds number is:

$$Re_p = \frac{\alpha_g d_s \rho_g |\vec{v}_s - \vec{v}_g|}{\mu_g} \qquad (A.4)$$

Syamlal and O'Brien(Syamlal and O'Brien, 1988) proposed a new drag coefficient based on the measurements of the terminal velocities of particles in the form

$$\beta = \frac{3}{4} C_d \frac{\alpha_s \rho_g}{d_s} \frac{\alpha_g}{f^2} |\vec{u}_g - \vec{u}_s| \qquad (A.5)$$

$$C_D = (0.63 + 4.8/\sqrt{f/Re_p})^2 \qquad (A.6)$$

where f is the ratio of the failing velocity of a suspension to the terminal velocity of a single particle.

$$f = \frac{1}{2}(A - 0.06 Re_p + \sqrt{((0.06 Re_p)^2 + 0.12 Re_p(2B - A) + A^2)}) \qquad (A.7)$$

with

$$A = \alpha_g^{4.14} \qquad (A.8)$$

$$B = \begin{cases} \alpha_g^{2.65} & \alpha_s < 0.15 \\ 0.8\alpha_g^{1.28} & \alpha_s \ge 0.15 \end{cases} \qquad (A.9)$$

Gibilaro et al.(Gibilaro *et al.*, 1985) considered an effective buoyancy force to produce drag coefficient correlation for individual particles in a fluidized suspension as follows:

$$\beta = [\frac{17.3}{Re_p} + 0.336]\frac{\rho_g}{d_s}|\vec{v}_s - \vec{v}_g|\alpha_s \alpha_g^{-1.8} \qquad (A.10)$$

McKeen and Pugsley et al.(McKeen and Pugsley, 2003) proposed an empirical method to reduce the Gibilaro(Gibilaro et al., 1985) drag correction using a constant scale factor K. This scale factor could be adjusted to take in to account the effect of interparticle cohesive forces on particle agglomeration.

$$\beta = K[\frac{17.3}{Re_p} + 0.336]\frac{\rho_g}{d_s}|\vec{v}_s - \vec{v}_g|\alpha_s \alpha_g^{-1.8} \qquad (A.11)$$